A&A, 686, A187 (2024)
https://doi.org/10.1051/0004-6361/202348996

Astronomy & Astrophysics

The ALPINE-ALMA [CII] survey: Dust emission effective radius up to 3 kpc in the early Universe

F. Pozzi[1,2], F. Calura[2], Q. D'Amato[1,3], M. Gavarente[1], M. Bethermin[4,5], M. Boquien[6], V. Casasola[7], A. Cimatti[1], R. Cochrane[8,9], M. Dessauges-Zavadsky[10], A. Enia[2], F. Esposito[1], A. L. Faisst[11], R. Gilli[2], M. Ginolfi[12,3], R. Gobat[13], C. Gruppioni[2], C. C. Hayward[9], E. Ibar[14], A. M. Koekemoer[15], B. C. Lemaux[16,17], G. E. Magdis[17,18,19], J. Molina[14], M. Romano[20,21], M. Talia[1], L. Vallini[2], D. Vergani[2], and G. Zamorani[2]

[1] Dipartimento di Fisica e Astronomia, Università di Bologna, Via Gobetti 93/2, 40129 Bologna, Italy
e-mail: f.pozzi@unibo.it
[2] INAF – Osservatorio di Astrofisica e Scienza dello Spazio di Bologna, Via Gobetti 93/3, 40129 Bologna, Italy
[3] INAF – Osservatorio Astrofisico di Arcetri Firenze, Via Largo Enrico Fermi 5, Firenze, Italy
[4] Université de Strasbourg, CNRS, Observatoire astronomique de Strasbourg, UMR 7550, 67000 Strasbourg, France
[5] Aix-Marseille Univ., CNRS, CNES, LAM, 13388 Marseille, France
[6] Université Côte d'Azur, Observatoire de la Côte d'Azur, CNRS, Laboratoire Lagrange, 06000 Nice, France
[7] INAF – Istituto di Radioastronomia Bologna, Via Gobetti 111, 40129 Bologna, Italy
[8] Department of Astronomy, Columbia University, New York, NY 10027, USA
[9] Center for Computational Astrophysics, Flatiron Institute, 162 Fifth Avenue, New York, NY 10010, USA
[10] Department of Astronomy, University of Geneva, Chemin Pegasi 51, 1290 Versoix, Switzerland
[11] Infrared Processing and Analysis Center, California Institute of Technology, Pasadena, CA 91125, USA
[12] Dipartimento di Fisica e Astronomia, Università degli Studi di Firenze, Via G. Sansone 1, 50019 Sesto Fiorentino, Firenze, Italy
[13] Instituto de Física, Pontificia Universidad Católica de Valparaíso, Casilla 4059, Valparaíso, Chile
[14] Instituto de Física y Astronomía, Universidad de Valparaíso, Avda. Gran Bretaña 1111, Valparaíso, Chile
[15] Space Telescope Science Institute, Baltimore, MD 21218, USA
[16] Department of Physics and Astronomy, University of California, Davis, One Shields Avenue, Davis, CA 95616, USA
[17] Cosmic Dawn Center (DAWN), Jagtvej 128, 2200 Copenhagen, N, Denmark
[18] DTU-Space, Technical University of Denmark, Elektrovej 327, 2800 Kgs. Lyngby, Denmark
[19] Niels Bohr Institute, University of Copenhagen, Jagtvej 128, 2200 Copenhagen N, Denmark
[20] National Centre for Nuclear Research, ul. Pasteura 7, 02-093 Warsaw, Poland
[21] INAF – Osservatorio Astronomico di Padova, Vicolo dell'Osservatorio 5, 35122 Padova, Italy

Received 18 December 2023 / Accepted 19 March 2024

ABSTRACT

Aims. Measurements of the size of dust continuum emission are an important tool for constraining the spatial extent of star formation, and hence the buildup of stellar mass. Compact dust emission has generally been observed at cosmic noon ($z \sim 2$–3). However, at earlier epochs, toward the end of the reionization ($z \sim 4$–6), only the sizes of a handful of infrared (IR) bright galaxies have been measured. In this work, we derive the dust emission sizes of main-sequence (MS) galaxies at $z \sim 5$ from the ALPINE survey.
Methods. We measured the dust effective radius, $r_{\rm e,FIR}$, in the *uv*-plane in Band 7 of ALMA for seven ALPINE galaxies with resolved emission and we compared it with rest-frame ultraviolet (UV) and [CII]158 µm measurements. We studied the $r_{\rm e,FIR}$–$L_{\rm IR}$ scaling relation by considering our dust size measurements and all the data in the literature at $z \sim 4$–6. Finally, we compared our size measurements with predictions from simulations.
Results. The dust emission in the selected ALPINE galaxies is rather extended ($r_{\rm e,FIR} \sim 1.5$–3 kpc), similar to [CII]158 µm but a factor of ∼2 larger than the rest-frame UV emission. Putting together all the measurements at $z \sim 5$, spanning two decades in luminosity from $L_{\rm IR} \sim 10^{11}\,L_{\odot}$ to $L_{\rm IR} \sim 10^{13}\,L_{\odot}$, the data highlight a steeply increasing trend of the $r_{\rm e,FIR}$–$L_{\rm IR}$ relation at $L_{\rm IR} < 10^{12}\,L_{\odot}$, followed by a downturn and a decreasing trend at brighter luminosities. Finally, simulations that extend up to the stellar masses of the ALPINE galaxies considered in the present work predict a subset of galaxies (∼25% at $10^{10}\,M_{\odot} < M_{\star} < 10^{11}\,M_{\odot}$) with sizes as large as those measured.

Key words. dust, extinction – galaxies: high-redshift – galaxies: ISM

1. Introduction

The size of dust continuum emission in the far IR (FIR) rest-frame regime gives key information on the spatial extension of the dust-obscured star formation within galaxies, and hence provides important constraints on their stellar buildup.

Nowadays, thanks to the Atacama Large Millimeter/Submillimeter array (ALMA), a significant number of studies of the FIR emission sizes have been performed at cosmic noon ($z \sim 2$) pointing toward compact dust emission (effective radius, $r_{\rm e,FIR} < 1$–2 kpc), typically more compact than the rest-frame optical or UV imaging (e.g., Barro et al. 2016; Tadaki et al. 2017; Talia et al. 2018; Franco et al. 2020). The compaction of the dust continuum sizes has been interpreted as a sign of dust-obscured buildup of a central dense stellar component, either through the secular funneling of gas toward the center (e.g.,

Dekel et al. 2013) or through gas-rich mergers (e.g., Puglisi et al. 2021). These studies focus mainly on dusty, massive, and FIR bright galaxies, while there are some hints that at fainter luminosities dust emission is more extended (e.g., Rujopakarn et al. 2016; Cheng et al. 2020; Romano et al. 2024).

At very high redshift, measuring the dust emission size is very challenging due to limited spatial resolution and sensitivity. Few studies are available for sources emerging shortly after the epoch of reionization ($4 < z < 6$). These studies include: Gómez-Guijarro et al. (2022a), who studied six sources in the GOODS-ALMA 2.0 survey at 1.1 mm; Jin et al. (2022), who considered six galaxies from the super-deblended catalogues in COSMOS and GOODS-North (Jin et al. 2018; Liu et al. 2018); and Cooke et al. (2018), in which the dust continuum sizes of six stacked luminous submillimeter galaxies are presented. These works support the very compact dust continuum sizes found at lower redshifts; however, the samples still rely on poor statistics and only the bright IR tail of galaxies has been probed ($L_{\rm IR}(8-1000\,\mu{\rm m}) > 10^{12}\,L_{\odot}$). An exception is the recent work from Witstok et al. (2022), which presents the properties of the Interstellar Medium (ISM) of five Lyman-break galaxies (LBGs) at very high z ($z \sim 7$), characterized by moderate IR luminosity ($L_{\rm IR} \sim 10^{11}\,L_{\odot}$).

We aim to improve our understanding of the dust emission sizes at high z ($4 < z < 6$) by taking advantage of the completed ALMA Large program to INvestigate [CII] at Early times (ALPINE, see Le Fèvre et al. 2020; Béthermin et al. 2020; Faisst et al. 2020). The goal of this program was to observe the prominent [CII] 158 μm line and FIR continuum emission of 118 normal, UV-selected star-forming galaxies at $z \sim 4.4-5.8$. The present study increases the number of sources with measured dust continuum sizes at very high z and, given the lower IR luminosity range spanned by the ALPINE galaxies, better constrains the $r_{\rm e,FIR}-L_{\rm IR}$ scaling relation.

The paper is organized as follows. In Sect. 2 we describe our data analysis. We then present our result in Sect. 3. Finally, we discuss them and conclude in Sect. 4. Throughout the paper, we assume a flat Lambda Cold Dark Matter (ΛCDM) cosmology with $\Omega_{\rm m} = 0.3$, $\Omega_{\lambda} = 0.7$ and $h_0 = 0.7$.

2. Sample, observations, and data analysis

The parent sample of galaxies analyzed in this paper is the subset of 23 objects with a ∼158 μm continuum detection in the ALPINE survey (Béthermin et al. 2020). The ALPINE survey aimed to study the ∼158 μm [CII] and the rest-frame FIR continuum emission of 118 MS rest-frame UV-selected galaxies at $z \sim 4.4-5.9$, in the COSMOS (Scoville et al. 2007) and ECDFS (Giacconi et al. 2002) fields. For an overall description of the survey we refer to Le Fèvre et al. (2020); for the data reduction we refer to Béthermin et al. (2020); and for the description of the ancillary spectra and photometric data and the physical properties obtained from the UV-to-optical Spectra Energy Distribution (SED) fitting, we refer to Faisst et al. (2020). The stellar masses ($M_{\star}$) and the star formation rates (SFRs) of the ALPINE galaxies are in the range of $M_{\star} = 10^{8.4}-10^{11}\,M_{\odot}$ and $1.5-270\,M_{\odot}\,{\rm yr}^{-1}$, respectively. The stellar masses, $M_{\star}$, are from Table A.1 of Faisst et al. (2020) and derived from the SED fitting. For the SFR, we considered ${\rm SFR_{UV+IR}}$; that is, the sum of the unobscured ($\rm SFR_{UV}$) and obscured ($\rm SFR_{IR}$) star formation. We derive $\rm SFR_{UV}$ from the UV luminosity at 1500 Å (Faisst et al. 2020) uncorrected for dust, and $\rm SFR_{IR}$ from the IR luminosity reported in Béthermin et al. (2020).

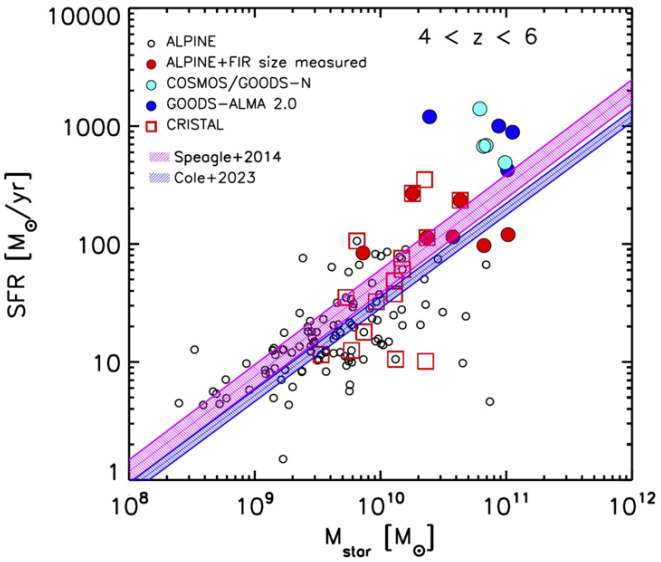

Fig. 1. SFR versus $M_{\star}$ for the ALPINE targets (red circles indicate galaxies with a FIR size measurement from the present work) and for our compilation of dust continuum measured sizes from the literature in a similar redshift range, $4 < z < 6$ (blue circles represent COSMOS/GOODS-North galaxies from super-deblended catalogues (Jin et al. 2022); cyan circles represent galaxies from the GOODS-ALMA 2.0 survey (Gómez-Guijarro et al. 2022a); and empty red squares represent galaxies from the CRISTAL survey (Mitsuhashi et al. 2023). For the CRISTAL sources that do not belong to the ALPINE survey, we used the SFR and $M_{\star}$ values reported in Table 1 of Mitsuhashi et al. (2023). The shaded violet region represents the 1σ range of the MS relation found by Cole et al. (2023) in the redshift range closer to the data ($4.5 < z < 5$) and obtained using the SFR values derived by averaging the star formation histories over 100 Myr timescales (see Table 2 in Cole et al. 2023); and the shaded pink region represents the MS relation and its 1σ dispersion found by Speagle et al. (2014) and computed, for consistency, at $z = 4.75$.

In Fig. 1 we report the ALPINE galaxies on the SFR–$M_{\star}$ plane. For the galaxies not detected in continuum, following Dessauges-Zavadsky et al. (2020), we considered only $\rm SFR_{UV}$. As was found by Schaerer et al. (2020) by studying the UV-continuum slope, this assumption can underestimate the total SFR by a factor of two. In Fig. 1, together with the ALPINE targets, we report the galaxies with measured continuum sizes in the redshift range $4 < z < 6$ (see Gómez-Guijarro et al. 2022a; Jin et al. 2022). Moreover, as a reference, we report the MS relation from Cole et al. (2023), recently derived using JWST data from Cosmic Evolution Early Release Science (CEERS, Finkelstein et al. 2022; Bagley et al. 2023) and consistent, within 1σ, with the pre-JWST derivation from Speagle et al. (2014). Of the 23 ALPINE continuum sources, three galaxies are classified in the continuum images as multicomponent objects (VC_5101209780,VE_530029038, DC_881725, see Béthermin et al. 2020). These systems could indicate the presence of a merger or a very patchy and disturbed galaxy where it can be quite difficult to constrain a center of the system and to determine the size. For this reason, we chose to remove these galaxies from our analysis. Therefore, our sample consists of 20 ALPINE galaxies. Among these 20 sources, 18 are detected in [CII], while for two sources only upper limits in [CII] are available.

In order to measure the continuum sizes of the targets, we adopted the procedure outlined in Fujimoto et al. (2020) to

Table 1. Summary of the key physical parameters of the galaxies explored in this work.

Name	z	$r_{e,FIR}$ [kpc]	$r_{e,[CII]}$ [kpc]	$r_{e,UV}$ [kpc]	$\log M_\star$ [$\log_{10}(M/M_\odot)$]	SFR [$M_\odot\,yr^{-1}$]	S/N
CG_19	4.500	<1.40	...	...	$9.83^{+0.07}_{-0.05}$	$66.5^{+13.5}_{-11.0}$	5.4
DC_396844	4.540	2.13 ± 1.10	2.56 ± 0.33	0.58 ± 0.20	$9.86^{+0.14}_{-0.19}$	$83.9^{+16.6}_{13.8}$	5.6
DC_488399	5.678	<1.17	1.32 ± 0.16	...	$10.20^{+0.13}_{-0.15}$	$89.8^{+14.9}_{-13.1}$	9.3
DC_494057	5.540	<1.16	2.48 ± 0.25	0.59 ± 0.17	$10.15^{+0.13}_{-0.15}$	$77.8^{+16.1}_{-13.8}$	7.1
DC_552206	5.514	3.08 ± 1.25	...	...	$10.58^{+0.14}_{-0.16}$	$114.9^{+29.6}_{-23.3}$	4.5
DC_683613[(a)]	5.536	<1.65	1.82 ± 0.33	0.57 ± 0.24	$10.17^{+0.14}_{-0.15}$	$75.6^{+18.6}_{-14.9}$	5.1
DC_818760[(a)]	4.554	2.70 ± 0.55	2.59 ± 0.16	1.07 ± 0.21[(b)]	$10.63^{+0.11}_{-0.10}$	$235.1^{+28.6}_{-25.5}$	9.5
DC_848185[(a)]	5.284	1.90 ± 0.30	...	...	$10.37^{+0.08}_{-0.19}$	$113.0^{+16.0}_{-14.3}$	7.1
DC_873756[(a)]	4.548	1.58 ± 0.20	2.36 ± 0.11	1.08 ± 0.43	$10.25^{+0.08}_{-0.10}$	$268.7^{+16.7}_{-15.5}$	21.7
VC_5100822662[(a)]	4.523	<1.16	2.59 ± 0.37	1.32 ± 0.33	$10.17^{+0.13}_{-0.14}$	$60.8^{+10.5}_{-9.0}$	6.5
VC_5101218326	4.568	1.83 ± 0.40	2.37 ± 0.15	1.46 ± 0.32	$11.01^{+0.07}_{-0.05}$	$120.0^{+18.0}_{-15.6}$	6.5
VC_5180966608	4.529	2.60 ± 0.60	No data	0.59 ± 0.24[(b)]	$10.82^{+0.12}_{-0.13}$	$96.9^{+19.5}_{-16.0}$	5.7

Notes. Column (1): ALPINE source name. We only list the 12 sources with a S/N of the continuum >4.5 (see Béthermin et al. 2020) that are considered in our analysis. The three sources classified in Béthermin et al. (2020) as multicomponent objects have not been considered. The [(a)] symbol indicates galaxies in common with the CRISTAL sample (Mitsuhashi et al. 2023). Column (2): spectroscopic redshift from the [CII] line emission. Column (3): dust continumm effective radius (see text for details). Column (4): [CII] line emission effective radius (Fujimoto et al. 2020). Column (5): rest-frame UV effective radius (Fujimoto et al. 2020). The [(b)] symbol indicates that the HST/$F160W$ map has been considered, otherwise the radius from the HST/$F814W$ maps have been reported. Columns (6) and (7): stellar mass and SFR (see text for details). Column (8): continuum S/N at 158 μm from Béthermin et al. (2020).

measure the sizes of the [CII] emission of the ALPINE targets. First of all, we remove from the visibility data the channels containing the [CII] emission. We then produce the continuum maps with the CASA[1](Bean 2022) task TCLEAN and we run in CASA the task IMFIT to achieve a first guess of the target's properties (positions, fluxes and sizes). These outputs, obtained in the image-plane, are used as first guess for the proper size measurements in the *uv*-plane, where we assume a 2D Gaussian model for the intensity profile and we measure the sizes with the CASA task UVMODELFIT. The latter returns the de-convolved FWHM along the major and minor axis ($FWHM_{maj}$, $FWHM_{min}$) that we circularize as $FWHM_{circ} = \sqrt{FWHM_{min} \times FWHM_{maj}}$). The effective radius r_e, which represents the radius that encloses half of the total light, is then derived as $r_e = FWHM_{circ}/2$ (see Voigt & Bridle 2010 for a Gaussian profile corresponding to a Sérsic index $n = 0.5$). Fujimoto et al. (2020) describe how a Gaussian profile return an effective radius r_{eff} consistent at a 5% level with a more reliable exponential shape (corresponding to a Sérsic index $n = 1$). We applied the described procedure to sources detected in the continuum at $S/N > 4.5$ to obtain reliable measurements. Given this cut in S/N, our final sample is composed of 12 galaxies. All but one of the 12 galaxies have continuum $S/N > 4.5$ (see Table 1), and this gives us confidence of meaningful size measurements (Fujimoto et al. 2020).

In Table 1 we report our size measurements. For 7 sources the fitting procedure returns a de-convolved FWHM along the minor and major axes, and we obtain a circularized effective radius ($r_{e,FIR}$). We also visually check the observed, model and residual maps in the image plane to exclude multicomponents below the scale of the beam (see Fig. 2). We note that for source DC_818760, constituted by three galaxies (see Jones et al. 2020; Devereaux et al. 2024), we measure and report the size of the central galaxy. For the remaining sources, since the fitting procedure reports de-convolved FWHM uncertainties larger or similar to the de-convolved FWHM measures, we estimate the size upper limit from the formula by Martí-Vidal et al. (2012) considering for the likelihood λ_c a value equal to 9 corresponding to a 3σ cut-off. We note that 3 resolved sources (DC_818760, DC_848185, DC_873756) are in common with the recent results from the CRISTAL survey (Mitsuhashi et al. 2023) and the size measurements are consistent within 1σ. Among the 5 unresolved sources, 2 sources (DC_683613, VC_5100822662) have a measured size in the CRISTAL sample consistent with our upper limits. The sources in common are highlighted in Table 1. In Table 1 along with $r_{e,FIR}$, we report the circularized effective radius of the [CII] line emission ($r_{e,[CII]}$) and of the rest-frame UV emission ($r_{e,UV}$). These radii were derived by Fujimoto et al. (2020) as follows: the [CII] radius from the ALMA ALPINE data using the CASA UVMODEL task described above; the rest-frame UV emission from the $F814W$ HST map (Koekemoer et al. 2007) and the $F160W$ HST maps (Koekemoer et al. 2011) using the GALFIT task (Peng et al. 2010). We only considered reliable size measurements (flag=0). Finally, in Table 1 we give the rest-frame optical radius $r_{e,opt}$ derived from the empirical stellar mass−size relation found recently by the JWST CEERS survey (Ward et al. 2024), given the stellar masses of our galaxies. We considered the mass−size relation in the redshift range closer to our data ($3.5 < z < 5$, see Table 1 in Ward et al. 2024).

3. Results

3.1. FIR, [CII] and UV sizes

In Fig. 3 we report the $r_{e,FIR}$ of the 12 ALPINE targets considered in this work with a $S/N > 4.5$ continuum detection (the upper limits of the unresolved sources are displayed as open circles). $r_{e,FIR}$ is presented in the left panel as a function of $M_\star$, in the middle panel as a function of the rest-frame UV sizes, $r_{e,UV}$, and of the optical radius, $r_{e,opt}$, derived by the JWST

[1] Common Astronomy Software Application: https://casa.nrao.edu/

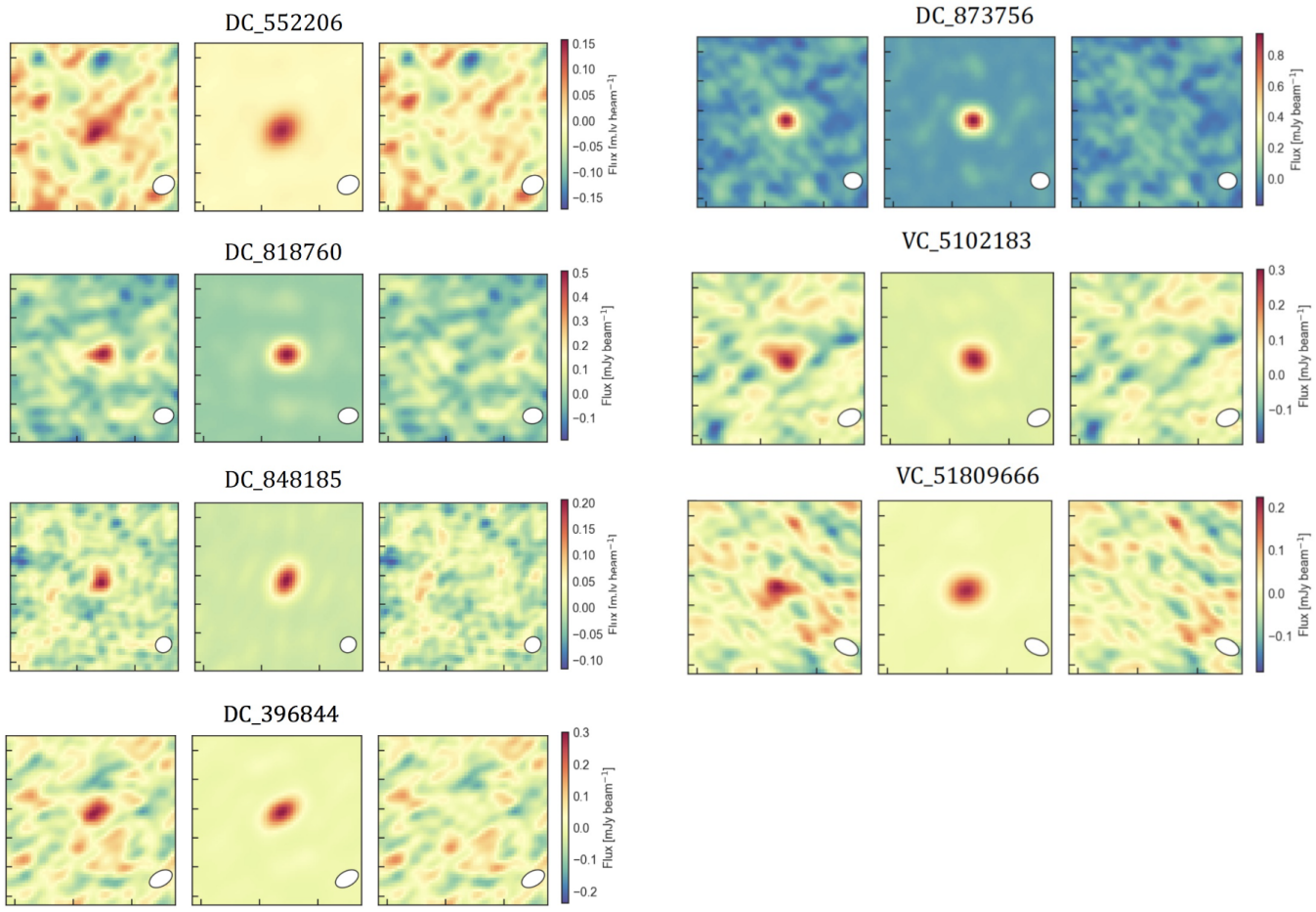

Fig. 2. Rest-frame FIR size measurements for the 7 resolved ALPINE sources using the CASA task UVMODELFIT. For every source, the three panels are, from left to right, the observed, modelled, and residual maps, respectively, all with a $10'' \times 10''$ size.

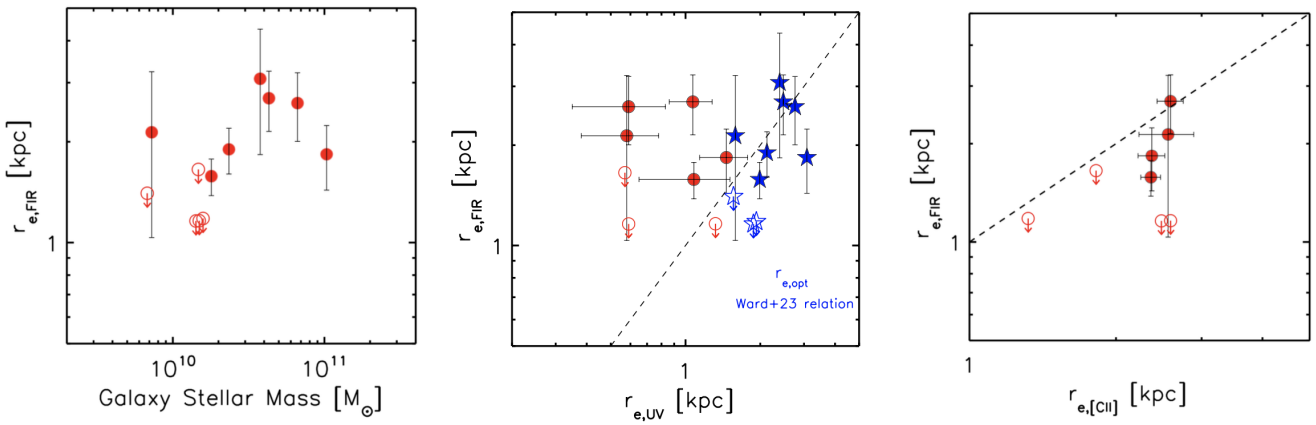

Fig. 3. Left: effective radius $r_{e,FIR}$ vs. stellar mass $M_\star$. Centre: $r_{e,FIR}$ vs. $r_{e,UV}$. The blue symbols represent the $r_{e,FIR}$ vs. the optical radius $r_{e,opt}$, with $r_{e,opt}$ from the empirical JWST mass−size relation (Ward et al. 2024) given the stellar masses of our sources. Right: $r_{e,FIR}$ vs. $r_{e,[CII]}$. The ALPINE galaxies continuum detected at $S/N > 4.5$ have been considered for the size analysis. The unresolved sources are reported as empty circles. Both $r_{e,UV}$ and $r_{e,[CII]}$ are from Fujimoto et al. (2020) and only the sources with a reliable measurements (flag = 0) have been considered.

stellar mass−size relation (Ward et al. 2024), and in the right panel as a function of the [CII] sizes, $r_{e,[CII]}$.

We find the median value to be $r_{e,FIR} = (2.13 \pm 0.26)$ kpc, and the ratios to be $r_{e,UV}/r_{e,FIR} = (0.39 \pm 0.15)$ and $r_{e,[CII]}/r_{e,FIR} = (1.29 \pm 0.14)$, calculated considering only the seven rest-frame FIR resolved sources and the 5(4) galaxies with measured $r_{e,UV}/r_{e,[CII]}$. The median ratio of the dust continuum sizes over the optical ones derived from the mass−size relation is $r_{e,opt}/r_{e,FIR} = 1.10 \pm 0.26$. The $r_{e,FIR}$ sizes are larger than those found for brighter FIR sources at similar redshifts (see the review from Hodge & da Cunha 2020 and references therein). They are slightly smaller than the [CII] sizes, tracing both the atomic and the molecular gas, and are significantly larger (by a factor of 2.5) than the rest-frame UV sizes, in contrast to what has been

found by other authors ($r_{e,HST}/r_{e,ALMA}$ = 1.6 for galaxies at $1 < z < 6$ taken from the ALMA archive by Fujimoto et al. 2017; $r_{e,HST}/r_{e,ALMA}$ = 2.3 for a compilation of massive galaxies at $z = 2–4$ in the GOODS-S by Franco et al. 2020) but in agreement with the results of the CRISTAL survey (Mitsuhashi et al. 2023). Moreover, our $r_{e,UV}/r_{e,FIR}$ are significant smaller (by up to a factor of 5–10) than the values predicted by the hydrodynamical cosmological simulations of Popping et al. (2022) and extrapolated at the stellar masses of our galaxies. This suggests that the model from Popping et al. (2022) could predict a too-compact FIR dust emission extension. Finally, we find that the dust continuum sizes are very close to the optical ones, as was predicted from the JWST mass−size relation, pointing toward a quite extended, disk-like star formation region traced by the IR emission, very similar to the region traced by the rest-frame optical emission. We will discuss in Sect. 3.2 our findings in comparison with other results from the literature and predictions from models.

3.2. Far-infrared sizes versus infrared luminosity and stellar masses

The study of scaling relations from IR data stands as a cornerstone in astrophysics, offering a comprehensive perspective on the properties of galaxies related to their coldest components; that is, neutral gas, molecular gas, and dust (Calura et al. 2017; Herrera-Camus et al. 2018; Casasola et al. 2020; Pastrav 2020). A poorly explored yet crucial quantity is the size of dust emission in high-redshift galaxies. In this work, we aim to leverage this essential parameter to investigate pivotal scaling relations; that is, the ones between size versus luminosity and size versus stellar mass.

In Fig. 4, we report our measures of $r_{e,FIR}$ as a function of the IR luminosity, L_{IR}. Here, L_{IR} has been computed from the rest-frame 158 μm emission by assuming the Béthermin et al. (2017) SED.

Together with our measurements, we report all the available rest-frame FIR size measurements from the literature at similar redshifts ($4 < z < 6$). To avoid bias introduced by the radial gradient in the dust temperature (e.g., Calistro Rivera et al. 2018; Cochrane et al. 2019), we considered galaxies observed at nearly the same wavelengths as the ALPINE galaxies (0.8−1 mm): this allowed us to sample the rest-frame continuum emission at the same frequencies, given the same redshift range. With blue symbols we show the measurements from the GOODS-ALMA 2.0 survey (Gómez-Guijarro et al. 2022a). The GOODS-ALMA 2.0 survey is an ALMA blind survey at 1.1 mm covering an area of 72.42 arcmin^2. The rest-frame FIR sizes were derived with a circular Gaussian model fit in the *uv*-plane, and combining the low- and high-resolution observations, leading to an average resolution of $0.447'' \times 0.418''$. Among the 88 blind detected sources in the GOODS-ALMA 2.0 survey, four sources satisfy our adopted selection criteria ($4 < z < 6$), with the redshift z estimated from photometry (Gómez-Guijarro et al. 2022a). In cyan symbols we report the dust continuum sizes of six galaxies from the super-deblended COSMOS and GOODS-North catalogues, selected for their very high photometric redshift ($z > 6$, Jin et al. 2022). Thanks to the detection of [CI](1–0) and CO transitions, the authors were able to measure the spectroscopic redshifts and, among the six sources, four sources satisfy our criteria ($4 < z < 6$). The dust continuum sizes are derived from 870 μm and 1 mm ALMA data.

We also report as open red squares the recent measurements of Mitsuhashi et al. (2023) from the CRISTAL survey (see Herrera-Camus et al., in prep. for the survey paper). The CRISTAL survey is composed of 24 target galaxies, of which 20 are from the ALPINE survey (five in common with the sample analyzed in the present work; see Table 1). This survey has been carried out at the same wavelengths as the ALPINE survey (Band 7: 0.8−1 mm), but at a higher spatial resolution (~0.3″). As is clear from Fig. 4, the CRISTAL sample probes the faintest galaxies studied so far, with FIR luminosities down to $L_{IR} \sim 10^{11}\,L_\odot$, while our data probe a luminosity domain scarcely populated by the dataset of Mitsuhashi et al. (2023). In this regard, the CRISTAL sample and the ALPINE dust continuum resolved sources from the present work are complementary. The analysis of a dataset that probes bright galaxies alongside another one probing fainter counterparts, all at similar redshifts, provides us with a comprehensive understanding, allowing us to characterize different trends of the $r_{e,FIR}-L_{IR}$ relation in distinct regimes of luminosity and size.

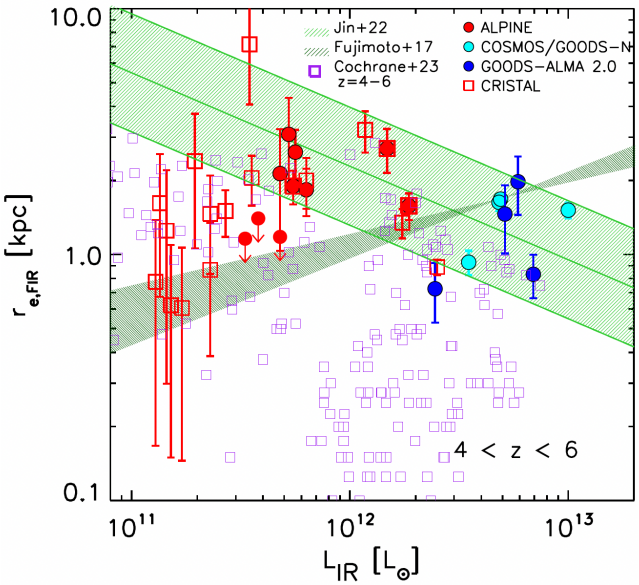

Fig. 4. Effective radius, $r_{e,FIR}$ vs. IR luminosity, L_{IR}, at $4 < z < 6$ for this sample and from the literature. Red circles represent the results of the ALPINE survey; blue circles the GOODS-ALMA 2.0 survey (Gómez-Guijarro et al. 2022a); cyan circles the super-deblended catalogs in the COSMOS and GOODS-North fields (Jin et al. 2022); and open red squares the CRISTAL survey (Mitsuhashi et al. 2023). The dark green shaded region represents the 1σ range of the relation found by Fujimoto et al. (2017). The green lines and the shaded region represent the relation and its 1σ dispersion found by Jin et al. (2022). The empty pink squares are simulation results from Cochrane et al. (2023) in the range $4 < z < 6$.

In Fig. 4, we report for comparison two relations: the one found by Fujimoto et al. (2017; dark green shaded region, representing the 1σ dispersion) and the one of Jin et al. (2022; green line, with its 1σ dispersion displayed as a shaded region). The result of Fujimoto et al. (2017) is based on a large sample of galaxies from the ALMA archive. Considering all the sources together ($0 < z < 6$), these authors find a positive correlation between $r_{e,FIR}$ and L_{IR} ($r_{e,FIR} \propto L_{IR}^{\alpha}$, with $\alpha = 0.28 \pm 0.07$).

This correlation is also confirmed by the authors in the highest redshift range considered ($2 < z < 4$). Fujimoto et al. (2017) discuss how the origin of the $r_{e,FIR}-L_{IR}$ relation could be related to the formation of stellar disks, since the IR slope is similar to the slope observed in the UV band, the latter explained by the predictions of disk formation models (i.e., van der Wel et al. 2014).

On the other hand, the relation from Jin et al. (2022) is based on a different compilation of measurements at $z > 1$: the six galaxies analyzed in their work, the galaxies from GOODS-ALMA (Franco et al. 2020; Gómez-Guijarro et al. 2022a), and a sample of MS galaxies at $z = 1-2$ (Valentino et al. 2020). Unlike Fujimoto et al. (2017), in the latter work the authors find an anticorrelation between the dust size and $L_{\rm IR}$ ($\log(FWHM$ size/kpc$) = -0.38 \times \log(L_{\rm IR}/10^{10}\,L_\odot) + 1.42$), indicating that galaxies with higher luminosities tend to have a more compact dust morphology.

In Fig. 4 we also show as empty pink squares the predictions from high-resolution, cosmological zoom-in simulations in a similar redshift range to that sampled by the data ($4 < z < 6$). These predictions are drawn from the FIRE (Hopkins et al. 2018) suite described in Cochrane et al. (2023) and were generated using the radiative transfer methods described by Cochrane et al. (2019), but extending the sample to lower FIR luminosities. To properly compare the model predictions to the data, we considered the observed-frame 850 μm emission sizes.

Concerning the data, a positive correlation between $r_{\rm e,FIR}$ and $L_{\rm IR}$ is supported at faint luminosities by the ALMA-CRISTAL data. On the other hand, across a luminosity range wider than 1 dex and extending from $L_{\rm IR} \sim 10^{11.5}\,L_\odot$ to $L_{\rm IR} = 2 \times 10^{13}\,L_\odot$, our measurements, together with the Jin et al. (2022) and Gómez-Guijarro et al. (2022b) data, support an anticorrelation between $r_{\rm e,FIR}$ and $L_{\rm IR}$, as was found by Jin et al. (2022), at odds with the results from Fujimoto et al. (2017). We are aware of the small number of galaxies with a measured dust continuum size at high z (>4) and high $L_{\rm IR}$ ($>10^{11.5}\,L_\odot$); anyway, we caution the reader of possible observational biases that may affect the Fujimoto et al. (2017) relation, given the sample inhomogeneity in terms of spatial resolution and sensitivity and the use of photometric redshift to derive sizes and $L_{\rm IR}$. Moreover, both the Jin et al. (2022) and Fujimoto et al. (2017) relations are obtained from samples including galaxies at lower z than the range considered in this work ($4 < z < 6$), and are both derived for IR bright galaxies ($L_{\rm IR} > 10^{11.4}$ and $>10^{12}\,L_\odot$, respectively).

Altogether, our results might suggest a variable trend of FIR luminosity as a function of size, which ranges from an increase for faint objects to a downturn at some characteristic luminosity on the order of $10^{12}\,L_\odot$, followed by a decreasing trend at brighter luminosities. A similar trend is shown also by the compilation of measures of Mitsuhashi et al. (2023), across a wider redshift range ($2 \le z \le 6$). The predictions of the zoom-in simulations (Cochrane et al. 2023) cover a broader range in dust continuum sizes than the data but, like the measurements, they present a characteristic IR luminosity around $10^{12}\,L_\odot$, above which the sizes decrease. Understanding the physical reason for this downturn and accounting for the characteristic luminosity value at which it occurs will be a major challenge for galaxy formation models.

In Fig. 5 we report our $r_{\rm e,FIR}$ as a function of the stellar mass, $M_\star$. As in Fig. 4, along with our measurements we show the other samples with dust continuum sizes measured in the literature at $z > 4$, from the GOODS-ALMA 2.0 survey (Gómez-Guijarro et al. 2022a), from the super deblended catalogues in the COSMOS and GOODS-North fields (Jin et al. 2022), and from the CRISTAL survey (Mitsuhashi et al. 2023).

In Fig. 5, together with the predictions from Cochrane et al. (2023; empty pink squares for galaxies in the range $4 < z < 6$), we also report the predictions from Popping et al. (2022; magenta and violet lines with shaded regions marking the 1σ scatter, for $z = 4$ and $z = 5$ galaxies, respectively). The predictions from Popping et al. (2022) are derived from the TNG50 simulations (Nelson et al. 2019; Pillepich et al. 2019), the highest-resolution implementation of the magnetohydrodynamical cosmological simulation IllustrisTNG (see Springel et al. 2018; Marinacci et al. 2018). For these predictions, we also considered the observed-frame 850 μm emission sizes. Results for galaxy stellar masses up to $\sim 10^{10.4}$ and $\sim 10^{11.4}\,M_\odot$ have been reported in the Popping et al. (2022) and Cochrane et al. (2019) simulations, respectively. The stellar mass range of our galaxies is not sampled in the volume of the Popping et al. (2022) simulation. At masses $<10^{10}\,M_\odot$, the model from Popping et al. (2022) predicts compact dust emission sizes (<1−2 kpc), similar to those observed in some CRISTAL galaxies (Mitsuhashi et al. 2023).

At masses $>10^{10}\,M_\odot$, a subset of model sources (~25% in the range $10^{10}\,M_\odot < M_\star < 10^{11}\,M_\odot$) from Cochrane et al. (2023) are predicted with large sizes, in the range of 1.5−4 kpc, populating the upper envelope of the distribution and in agreement with the ALPINE galaxies analyzed in the present work.

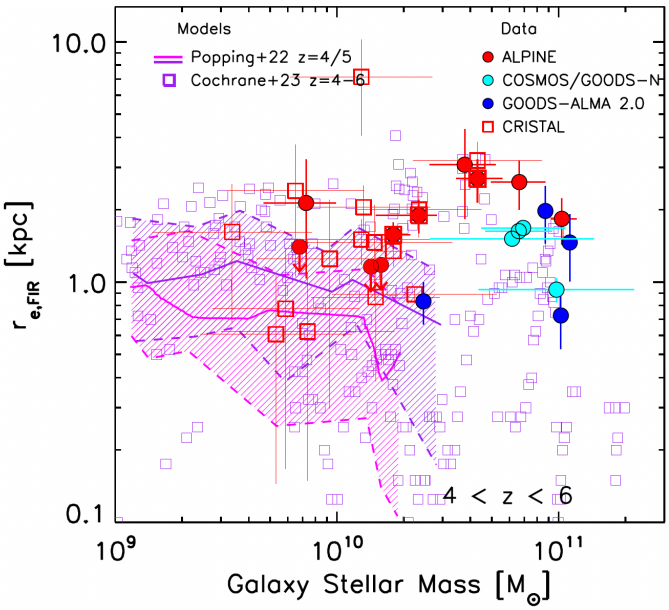

Fig. 5. Effective radius, $r_{\rm e,FIR}$, vs. stellar mass, $M_\star$, at $4 < z < 6$ for this sample and from the literature. The symbols are as in Fig. 4. Magenta and violet lines (with shaded regions marking the 1σ scatter) represent the predictions from Popping et al. (2022) for $z = 4$ and for $z = 5$ galaxies, respectively; empty pink squares are the predictions from Cochrane et al. (2023) in the range $4 < z < 6$.

4. Discussion and summary

Our study of the MS ALPINE galaxies at $z \sim 5$ shows an effective radius, $r_{\rm e,FIR}$, of 1.5−3 kpc, a factor of two larger than what is observed in brighter IR sources at similar z. We confirm, in fact, the anticorrelation found by Jin et al. (2022) between the dust size and the IR luminosity in the $L_{\rm IR}$ range between $\sim 10^{11.5}\,L_\odot$ and $\sim 2 \times 10^{13}\,L_\odot$. A possible explanation for the anticorrelation is ascribed to galaxies caught at different phases of their star formation history, all within the scatter of the MS (e.g., Sommovigo et al. 2021; Gómez-Guijarro et al. 2022b; Vallini et al. 2024). In this picture, the ALPINE galaxies are characterized by a mild SFR and a more extended (possibly disk-like) star formation region, while IR brighter galaxies are characterized by an enhanced SFR, a short depletion time, and

high dust temperatures. To validate this scenario, we considered the depletion times ($t_{\rm depl}$) and the gas fractions ($f_{\rm gas} = \frac{M_{\rm gas}}{M_\star + M_{\rm gas}}$) of the ALPINE galaxies with a measured dust size, derived by Dessauges-Zavadsky et al. (2020) from the [CII] luminosities: $t_{\rm depl} = (456 \pm 57)$ Myr and $f_{\rm gas} = 0.6 \pm 0.2$. These values are in agreement with those derived from Gómez-Guijarro et al. (2022b) for normal star-forming galaxies with an extended star-forming region, as opposed to the typical values of starburst galaxies, characterized by a more compact emission, shorter $t_{\rm depl}$ (on the order of 10–100 Myr; see also Silverman et al. 2015; Scoville et al. 2023) and a lower gas fraction (in the range of 0.25–0.5; see Fig. 3 in Gómez-Guijarro et al. 2022b). Our finding is in line with the recent result obtained by Béthermin et al. (2023) on the Kennicutt–Schmidt (KS) relation at $z \sim 4.5$: they analyzed four galaxies (three in common with the present sample) at a higher spatial resolution ($0.2''-0.3''$), showing how MS galaxies have significantly lower $\Sigma_{\rm SFR}$, at a given $\Sigma_{\rm gas}$, in comparison to high-z starburst galaxies.

On the other hand, in fainter galaxies, the new CRISTAL sample (Mitsuhashi et al. 2023) supports a positive correlation between IR size and IR luminosity. Altogether, the data samples considered in this work, spanning 2 dex in IR luminosity, highlight a variable trend in the $r_{\rm e,FIR}-L_{\rm IR}$ relation, ranging from steeply increasing behavior at $L_{\rm IR} < 10^{12}\,L_\odot$, followed by a downturn and a decreasing trend at brighter luminosities.

Finally, we compare our dust emission sizes with the cosmological simulations of Cochrane et al. (2023) and Popping et al. (2022). Their results suggest smaller dust continuum sizes than our measurements but in Cochrane et al. (2023), the only simulation that extends up to our stellar masses, a tail of sizes as large as those observed in the ALPINE galaxies is predicted.

Future ALMA observations at a higher resolution and in different bands will strengthen this result by enlarging the sample of galaxies with a measured size and by allowing the estimate of another key parameter: the dust temperature. Besides being crucial in the estimation of the dust mass (e.g., Bianchi 2013; Pozzi et al. 2021), this quantity is critically sensitive to the optical thickness of the dust-emitting region (e.g., Jin et al. 2022) and to the source physical area (hence its size Gilli et al. 2022). Further elucidating the scaling relations presented here by means of improved observations and better understanding the underlying physical mechanisms are important avenues for future investigation, and will provide fundamental insights in future galaxy evolution studies.

Acknowledgements. This paper is dedicated to the memory of Olivier Le Fèvre, PI of the ALPINE survey. We thank the referee for their in-sightful comments. We acknowledge support from grant PRIN MIUR 2017- 20173ML3WW_s. FP, VC, FE and FC acknowledge funding from the INAF Mini Grant 2022 program "Face-to-Face with the Local Universe: ISM's Empowerment (LOCAL)". FC acknowledges support from the INAF main-stream (1.05.01.86.31). EI acknowledges funding by ANID FONDECYT Regular 1221846. GEM acknowledges the Villum Fonden research grant 13160 "Gas to stars, stars to dust: tracing star formation across cosmic time", grant 37440, "The Hidden Cosmos", and the Cosmic Dawn Center of Excellence funded by the Danish National Research Foundation under the grant No. 140. MB acknowledges support from the French government through the France 2030 investment plan managed by the National Research Agency (ANR), as part of the Initiative of Excellence of Université Côte d'Azur under reference number ANR-15-IDEX-01. MR acknowledges support from the Narodowe Centrum Nauki (UMO-2020/38/E/ST9/00077) and support from the Foundation for Polish Science (FNP) under the program START 063.2023.

References

Bagley, M. B., Finkelstein, S. L., Koekemoer, A. M., et al. 2023, ApJ, 946, L12
Barro, G., Kriek, M., Pérez-González, P. G., et al. 2016, ApJ, 827, L32
Béthermin, M., Wu, H.-Y., Lagache, G., et al. 2017, A&A, 607, A89
Béthermin, M., Fudamoto, Y., Ginolfi, M., et al. 2020, A&A, 643, A2
Béthermin, M., Accard, C., Guillaume, C., et al. 2023, A&A, 680, L8
Bianchi, S. 2013, A&A, 552, A89
Calistro Rivera, G., Hodge, J. A., Smail, I., et al. 2018, ApJ, 863, 56
Calura, F., Pozzi, F., Cresci, G., et al. 2017, MNRAS, 465, 54
Bean, B. 2022, PASP, 134, 114501
Casasola, V., Bianchi, S., De Vis, P., et al. 2020, A&A, 633, A100
Cheng, C., Ibar, E., Smail, I., et al. 2020, MNRAS, 499, 5241
Cochrane, R. K., Hayward, C. C., Anglés-Alcázar, D., et al. 2019, MNRAS, 488, 1779
Cochrane, R. K., Hayward, C. C., Anglés-Alcázar, D., & Somerville, R. S. 2023, MNRAS, 518, 5522
Cole, J. W., Papovich, C., Finkelstein, S. L., et al. 2023, arXiv e-prints [arXiv:2312.10152]
Cooke, E. A., Smail, I., Swinbank, A. M., et al. 2018, ApJ, 861, 100
Dekel, A., Zolotov, A., Tweed, D., et al. 2013, MNRAS, 435, 999
Dessauges-Zavadsky, M., Ginolfi, M., Pozzi, F., et al. 2020, A&A, 643, A5
Devereaux, T., Cassata, P., Ibar, E., et al. 2024, A&A, 686, A156
Faisst, A. L., Schaerer, D., Lemaux, B. C., et al. 2020, ApJS, 247, 61
Finkelstein, S. L., Bagley, M. B., Arrabal Haro, P., et al. 2022, ApJ, 940, L55
Franco, M., Elbaz, D., Zhou, L., et al. 2020, A&A, 643, A30
Fujimoto, S., Ouchi, M., Shibuya, T., & Nagai, H. 2017, ApJ, 850, 83
Fujimoto, S., Silverman, J. D., Bethermin, M., et al. 2020, ApJ, 900, 1
Giacconi, R., Zirm, A., Wang, J., et al. 2002, ApJS, 139, 369
Gilli, R., Norman, C., Calura, F., et al. 2022, A&A, 666, A17
Gómez-Guijarro, C., Elbaz, D., Xiao, M., et al. 2022a, A&A, 658, A43
Gómez-Guijarro, C., Elbaz, D., Xiao, M., et al. 2022b, A&A, 659, A196
Herrera-Camus, R., Sturm, E., Graciá-Carpio, J., et al. 2018, ApJ, 861, 95
Hodge, J. A., & da Cunha, E. 2020, Royal Soc. Open Sci., 7, 200556
Hopkins, P. F., Wetzel, A., Kereš, D., et al. 2018, MNRAS, 480, 800
Jin, S., Daddi, E., Liu, D., et al. 2018, ApJ, 864, 56
Jin, S., Daddi, E., Magdis, G. E., et al. 2022, A&A, 665, A3
Jones, G. C., Béthermin, M., Fudamoto, Y., et al. 2020, MNRAS, 491, L18
Koekemoer, A. M., Aussel, H., Calzetti, D., et al. 2007, ApJS, 172, 196
Koekemoer, A. M., Faber, S. M., Ferguson, H. C., et al. 2011, ApJS, 197, 36
Le Fèvre, O., Béthermin, M., Faisst, A., et al. 2020, A&A, 643, A1
Liu, D., Daddi, E., Dickinson, M., et al. 2018, ApJ, 853, 172
Marinacci, F., Vogelsberger, M., Pakmor, R., et al. 2018, MNRAS, 480, 5113
Martí-Vidal, I., Pérez-Torres, M. A., & Lobanov, A. P. 2012, A&A, 541, A135
Mitsuhashi, I., Tadaki, K. I., Ikeda, R., et al. 2023, arXiv e-prints [arXiv:2311.17671]
Nelson, D., Pillepich, A., Springel, V., et al. 2019, MNRAS, 490, 3234
Pastrav, B. A. 2020, MNRAS, 493, 3580
Peng, C. Y., Ho, L. C., Impey, C. D., & Rix, H.-W. 2010, AJ, 139, 2097
Pillepich, A., Nelson, D., Springel, V., et al. 2019, MNRAS, 490, 3196
Popping, G., Pillepich, A., Calistro Rivera, G., et al. 2022, MNRAS, 510, 3321
Pozzi, F., Calura, F., Fudamoto, Y., et al. 2021, A&A, 653, A84
Puglisi, A., Daddi, E., Valentino, F., et al. 2021, MNRAS, 508, 5217
Romano, M., Donevski, D., Junais, A., et al. 2024, A&A, 683, L9
Rujopakarn, W., Dunlop, J. S., Rieke, G. H., et al. 2016, ApJ, 833, 12
Schaerer, D., Ginolfi, M., Béthermin, M., et al. 2020, A&A, 643, A3
Scoville, N., Aussel, H., Brusa, M., et al. 2007, ApJS, 172, 1
Scoville, N., Faisst, A., Weaver, J., et al. 2023, ApJ, 943, 82
Silverman, J. D., Daddi, E., Rodighiero, G., et al. 2015, ApJ, 812, L23
Sommovigo, L., Ferrara, A., Carniani, S., et al. 2021, MNRAS, 503, 4878
Speagle, J. S., Steinhardt, C. L., Capak, P. L., & Silverman, J. D. 2014, ApJS, 214, 15
Springel, V., Pakmor, R., Pillepich, A., et al. 2018, MNRAS, 475, 676
Tadaki, K.-I., Genzel, R., Kodama, T., et al. 2017, ApJ, 834, 135
Talia, M., Pozzi, F., Vallini, L., et al. 2018, MNRAS, 476, 3956
Valentino, F., Magdis, G. E., Daddi, E., et al. 2020, ApJ, 890, 24
Vallini, L., Witstok, J., Sommovigo, L., et al. 2024, MNRAS, 527, 10
van der Wel, A., Franx, M., van Dokkum, P. G., et al. 2014, ApJ, 788, 28
Voigt, L. M., & Bridle, S. L. 2010, Limitations of Model-fitting Methods for Lensing Shear Estimation (Oxford: Oxford University Press)
Ward, E., de la Vega, A., Mobasher, B., et al. 2024, ApJ, 962, 176
Witstok, J., Smit, R., Maiolino, R., et al. 2022, MNRAS, 515, 1751